BIOCHEMISTRY
including biophysical chemistry & molecular biology

Article

pubs.acs.org/biochemistry

Atomic Force Microscopy Imaging Reveals the Domain Structure of Polycystin-1

Peter Oatley,[†] Andrew P. Stewart,[†] Richard Sandford,[‡] and J. Michael Edwardson*[,†]

[†]Department of Pharmacology, University of Cambridge, Tennis Court Road, Cambridge CB2 1PD, U.K.

[‡]Department of Medical Genetics, Cambridge Institute for Medical Research, Addenbrooke's Hospital, Cambridge CB2 0XY, U.K.

Supporting Information

ABSTRACT: Mutation of polycystin-1 (PC1) is the major cause of autosomal dominant polycystic kidney disease. PC1 has a predicted molecular mass of ~460 kDa comprising a long multidomain extracellular N-terminal region, 11 transmembrane regions, and a short C-terminal region. Because of its size, PC1 has proven difficult to handle biochemically, and structural information is consequently sparse. Here we have isolated wild-type PC1, and several mutants, from transfected cells by immunoaffinity chromatography and visualized individual molecules using atomic force microscopy (AFM) imaging. Full-length PC1 appeared as two unequally sized blobs connected by a 35 nm string. The relative sizes of the two blobs suggested that the smaller one represents the N-terminus, including the leucine-rich repeats, the first polycystic kidney disease (PKD) domain, and the C-type lectin motif, while the larger one is the C-terminus, including the receptor for egg jelly (REJ) domain, all transmembrane domains, and the cytoplasmic tail. The intervening string would then consist of a series of tandem PKD domains. The structures of the various PC1 mutants were all consistent with this model. Our results represent the first direct visualization of the structure of PC1, and reveal the architecture of the protein, with intriguing implications for its function.

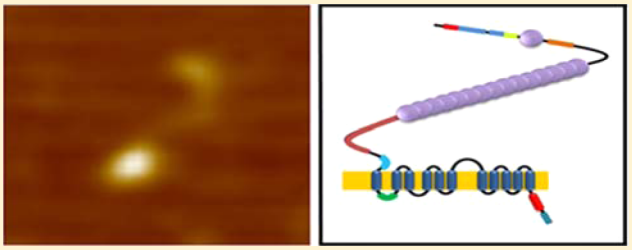

Autosomal dominant polycystic kidney disease (ADPKD) is one of the most common inherited human disorders (reviewed in refs 1−3), with a population prevalence of over 1:1000. ADPKD is characterized by the progressive development of multiple fluid-filled cysts derived from renal tubular epithelial cells and is a leading cause of end-stage renal failure. It is caused by mutations in two genes, *PKD1*[4,5] and *PKD2*.[6] The proteins encoded by these genes, polycystin-1 (PC1) and polycystin-2 (PC2), have been reported to form a Ca^{2+}-permeable ion channel complex.[7] This complex, present on the renal primary cilium[8−10] (reviewed in ref 11), is believed to be activated by extracellular mechanical stimuli such as fluid flow and regulates multiple intracellular signaling pathways.[7,12] In addition, PC2 (also known as TRPP2, a member of the TRP channel protein superfamily) appears to have a role, independent of PC1, in regulating Ca^{2+} efflux from the endoplasmic reticulum (ER[13,14]).

PC1 is a very large (4293 amino acids) protein with a long (>3000 amino acids) extracellular N-terminal region, 11 transmembrane regions, and a relatively short (225 amino acids) C-terminal region (Figure 1). Exogenously expressed PC1 typically migrates on gels as a protein of molecular mass ~500 kDa (e.g., ref 15), although the native, fully glycosylated protein has a molecular mass of ~600 kDa.[16] The extracellular region of PC1 contains several putative structural domains, including a leucine-rich repeat flanked by two cysteine-rich domains, a "cell wall integrity and stress response component" or WSC domain, a C-type lectin domain, 16 immunoglobulin-like PKD domains (15 of them in tandem), and, close to the membrane, an ~1000-amino acid receptor for egg jelly (REJ) domain. Between the REJ domain and the first transmembrane domain is an ~50-amino acid G protein-coupled receptor proteolytic site (GPS), at which cellular PC1 can be cleaved via

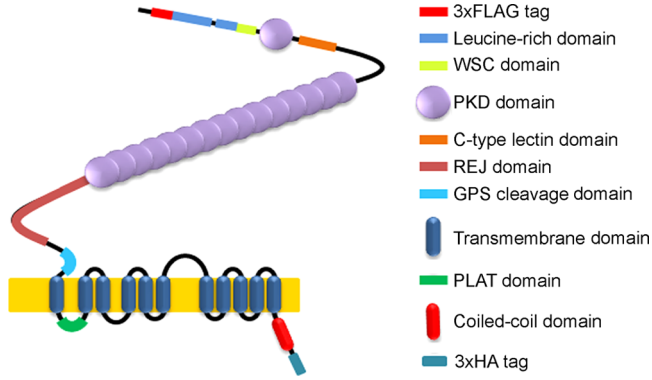

Figure 1. Schematic illustration of the domain architecture of PC1. GPS, G protein-coupled receptor proteolytic site; PKD, polycystic kidney disease; PLAT, polycystin−lipoxygenase−alphatoxin; REJ, receptor for egg jelly; WSC, cell wall integrity and stress response component.

Received: January 30, 2012
Revised: March 8, 2012
Published: March 12, 2012

   dx.doi.org/10.1021/bi300134b | *Biochemistry* 2012, 51, 2879−2888

cis-autoproteolysis,[17] leaving the N-terminal fragment (NTF) and the C-terminal fragment (CTF) attached to each other noncovalently.[15] The first intracellular loop within the membrane-associated region contains a polycystin−lipoxygenase−alphatoxin (PLAT) domain. Finally, the cytoplasmic C-terminal region contains a putative coiled-coil region that appears to be involved in the interaction of PC1 with PC2.[18,19]

PC1 undergoes cleavage during its movement through the secretory pathway. This occurs at the GPS cleavage site, as mentioned above.[15] Cleavage at this site begins shortly after protein synthesis but does not proceed to completion—typically approximately half of the protein remains uncleaved.[20] Interestingly, a comparison of the phenotypes of PC1 knockout mice and knock-in mice expressing noncleavable PC1 indicates that cleaved and uncleaved PC1 perform distinct functions.[20] Two additional cleavage events occur within the C-terminal tail of PC1, releasing fragments that enter the nucleus and regulate cell signaling pathways.[21,22] The extent of these C-terminal cleavage events depends on the rate of renal tubular fluid flow, suggesting that the generation of the cytoplasmic fragments contributes to the proposed role of PC1 in mechanosensation within the tubule.[21]

Because of its size, PC1 has proven to be very difficult to handle biochemically, and structural information is consequently sparse. In the present study, we set out to isolate PC1 from transiently transfected cells and image it using atomic force microscopy (AFM). By imaging WT PC1 and a group of mutants at the single-molecule level, we have been able to provide the first glimpse of the structure of this protein and to map the positions of its constituent regions.

MATERIALS AND METHODS

Constructs. The WT mouse PC1 construct in the pcDNA3.1 vector (Invitrogen) has a triple FLAG tag close to the N-terminus (after the first 27 amino acids, including the signal sequence) and a triple HA tag at the C-terminus.[23] The PC1 GPS cleavage mutant is identical except for an L3040H mutation.[17] Both constructs were kindly provided by Dr. M. J. Caplan (Yale University, New Haven, CT). Two additional mutants with differently sized deletions in the extracellular region were generated in the GPS cleavage mutant background: deletion mutant 1, Δ1188−2103, created using restriction enzymes *Hpa*I and EcoRV, and deletion mutant 2, Δ1118−2691, created using FspAI.

Transient Transfection of tsA 201 Cells. tsA 201 cells (a subclone of human embryonic kidney-293 cells stably expressing the SV40 large T-antigen) were grown in Dulbecco's modified Eagle's medium supplemented with 10% (v/v) fetal calf serum, 100 units/mL penicillin, and 100 μg/mL streptomycin, in an atmosphere of 5% CO_2/air. Transient transfections of tsA 201 cells with DNA were carried out using the calcium phosphate method, with reagents prepared in-house. Protein expression and intracellular localization were checked using immunofluorescence analysis. Nontransfected cells were used as a negative control. Cells were fixed, permeabilized, and incubated with either mouse monoclonal anti-HA (Covance) or mouse monoclonal anti-FLAG (Sigma) primary antibodies, followed by Cy3-conjugated goat secondary antibodies (Sigma). Cells were imaged by confocal laser scanning microscopy. As shown in the Supporting Information, Figure S1, both FLAG and HA tags were detected on all four constructs, and the staining pattern indicated that the constructs were predominantly in intracellular compartments.

Solubilization and Isolation of Epitope-Tagged Proteins. A total of 250 μg of DNA was used to transfect cells in 5 × 162 cm^2 culture flasks. After transfection, cells were incubated for 48 h to allow protein expression. A crude membrane fraction of transfected cells was solubilized in 1% Triton X-100 for 1 h before centrifugation at 61740*g* to remove insoluble material. To isolate PC1, the solubilized extract was incubated with either anti-HA or anti-FLAG agarose beads (Sigma) for 3 h. The beads were washed extensively, and bound proteins were eluted with HA or FLAG peptide (300 μg/mL). In all cases, samples were analyzed by SDS−polyacrylamide gel electrophoresis, and proteins were detected by both silver staining and by immunoblotting with appropriate antibodies (see above). For proteomic analysis silver stained bands were excised from the gel and analyzed by orbitrap mass spectrometry.

AFM Imaging. Isolated proteins were diluted, and 45 μL of the sample was allowed to adsorb to freshly cleaved, poly(L-lysine)-coated mica disks. After a 5 min incubation, the sample was washed with BPC-grade water (Sigma) and dried under nitrogen. Imaging was performed with a Veeco Digital Instruments Multimode AFM controlled by a Nanoscope IIIa controller. Samples were imaged in air, using tapping mode. The silicon cantilevers used had a drive frequency ∼300 kHz and a specified spring constant of 40 N/m (Olympus). The applied imaging force was kept as low as possible ($A_s/A_0 \sim 0.85$).

The molecular volumes of the protein particles were determined from particle dimensions based on AFM images. After adsorption of the proteins onto the mica support, the particles adopted the shape of a spherical cap. Scanning Probe Image Processor (SPIP) Version 5 (Image Metrology) was used to measure particle height (Z-Max) and diameter. It is well-known that the geometry of the scanning AFM probe introduces a tendency to overestimate particle diameter. To minimize this probe convolution error, we used an SPIP particle threshold of 0.3 nm to provide accurate measurements of diameter. This value was chosen after comparing the volumes calculated manually for immunoglobulin G molecules with the volumes generated using SPIP and with the predicted volume, based on molecular mass.

Molecular volume was calculated using the equation

$$V_m = (\pi h/6)(3r^2 + h^2) \quad (1)$$

where h is the particle height and r is the radius. Molecular volume based on molecular mass was calculated using the equation

$$V_c = (M_0/N_0)(V_1 + dV_2) \quad (2)$$

where M_0 is the molecular mass, N_0 is Avogadro's number, V_1 and V_2 are the partial specific volumes of particle (0.74 cm^3/g) and water (1 cm^3/g), respectively, and d is the extent of protein hydration (taken as 0.4 g water/g protein).

Note that it has been shown previously[24] that the molecular volumes of proteins measured by imaging in air are similar to the values obtained by imaging under fluid; hence, the process of drying does not significantly affect the measured molecular volume. It has also been shown by us[25] and by others[24] that there is a close correspondence between the measured and predicted molecular volumes for various proteins over a wide range of molecular masses; hence, molecular volume is measured reasonably accurately by AFM imaging.

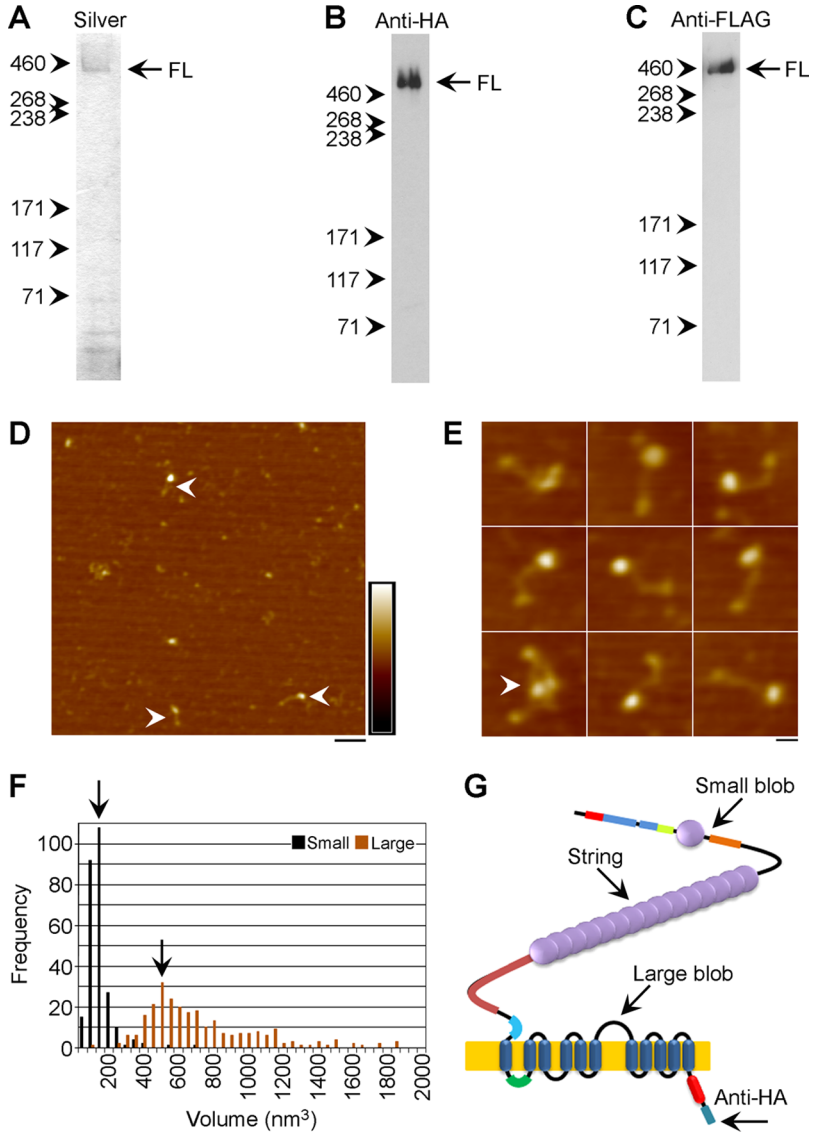

Figure 2. Isolation and AFM imaging of PC1 GPS cleavage mutant. Protein was isolated from a detergent extract of a crude membrane fraction from transfected cells by immunoaffinity chromatography, using anti-HA immunobeads, followed by elution with HA peptide. Isolated protein was analyzed by silver staining (A) or immunoblotting using mouse monoclonal anti-HA (B) or anti-FLAG (C) antibodies, followed by horseradish peroxidase conjugated goat anti-mouse secondary antibody. Immunoreactive bands were detected using enhanced chemiluminescence. (D) Low-magnification AFM image of isolated proteins. Characteristic structures, consisting of unequally sized blobs connected by strings, are indicated by the arrowheads. Horizontal scale bar, 100 nm. Color-height scale, 0–5 nm. (E) Gallery of zoomed images of blob–string–blob structures. Two proteins that appear to have undergone self-association are indicated by an arrowhead. Horizontal scale bar, 25 nm. (F) Frequency distributions of molecular volumes of small and large blobs. Arrows indicate volume peaks. (G) Schematic illustration of the isolated protein, indicating the epitope tag used for affinity purification. Arrows indicate the proposed components of the imaged structures.

Data Analysis. Data were separated into appropriate bin widths and histograms plotted. Using SigmaPlot version 10.0, Gaussian curves were fitted and the mean value of the peaks calculated. Welch's *t*-tests of unequal sample size and unequal variance were used to determine if the mean particle volumes were significantly different from each another.

RESULTS

Purification and AFM Imaging of the PC1 GPS Cleavage Mutant. We began our investigation with the mouse PC1 GPS cleavage mutant (L3040H[17]) in order to circumvent complications arising from endogenous cleavage of the protein.[15] This construct, with a triple FLAG tag close to the N-terminus and a triple hemagglutinin (HA) tag at the C-terminus, was isolated from transfected tsA 201 cells by immunoaffinity chromatography using anti-HA immunobeads. Protein eluted from the beads by incubation with the HA peptide was subjected to SDS–polyacrylamide gel electrophoresis followed by silver staining and immunoblotting using either anti-HA or anti-FLAG antibodies. The silver stain showed a prominent band at a molecular mass of ~460 kDa, consistent with the known size of full-length (FL) PC1 (Figure 2A). Several minor contaminants were also visible close to or below the 71 kDa marker. Proteomic analysis indicated that the two major contaminants were the 78 kDa glucose-regulated protein and the 70 kDa heat shock protein 1A. Both of these proteins are believed to have chaperoning roles during protein folding and assembly in the ER. The ~460 kDa band could be

dx.doi.org/10.1021/bi300134b | *Biochemistry* 2012, 51, 2879–2888

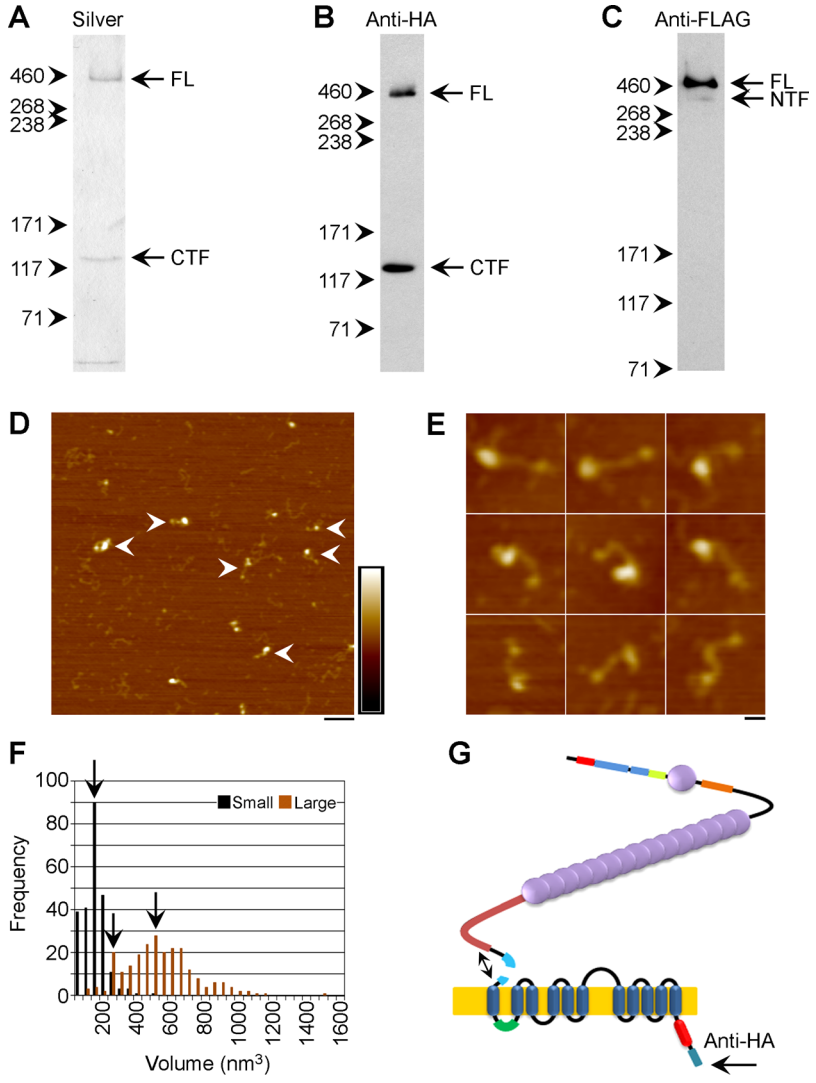

Figure 3. AFM imaging of WT PC1 isolated using anti-HA immunobeads. Protein was isolated by immunoaffinity chromatography, using anti-HA immunobeads, followed by elution with HA peptide. Isolated protein was analyzed by silver staining (A) or immunoblotting using mouse monoclonal anti-HA (B) or anti-FLAG (C) antibodies. (D) Low-magnification AFM image of isolated proteins. Blob–string–blob structures are indicated by the arrowheads. Horizontal scale bar, 100 nm. Color-height scale, 0–5 nm. (E) Gallery of zoomed images of blob–string–blob structures. Horizontal scale bar, 25 nm. (F) Frequency distributions of molecular volumes of small and large blobs. Arrows indicate volume peaks. (G) Schematic illustration of the isolated protein, indicating the epitope tag used for affinity purification.

decorated by either anti-HA (Figure 2B) or anti-FLAG antibodies (Figure 2C), confirming that it was indeed FL PC1.

Isolated PC1 GPS cleavage mutant was imaged by AFM in air. A typical low-magnification image is shown in Figure 2D. Several structures can be seen that consist of two unequally sized blobs connected by a string (arrowheads). A gallery of zoomed images of the isolated proteins is shown in Figure 2E. The arrowhead in the bottom left-hand panel in Figure 2E indicates a pair of PC1 molecules that have self-associated. These interactions were rare, and we cannot exclude the possibility that they are an artifact of the purification/incubation procedure. A number of the structures were identified, and the molecular volumes of the two blobs in each structure were measured, using eq 1. Statistical analysis of Gaussian fits of the volume data indicated the presence of two populations of particles. Consequently, for each structure, the smaller and larger of the two blobs were assigned to separate particle groups. Frequency distributions of the measured molecular volumes in the two groups are shown in Figure 2F. The mean volumes of separate Gaussian fits for the smaller and larger particles were 105 ± 1 (SEM) nm^3 and 544 ± 15 nm^3 (n = 259 for each), respectively. According to eq 2, these volumes represent approximate molecular masses of 56 and 228 kDa, respectively. These masses are close to the predicted masses of 554 amino acids at the N-terminus, which would include the two leucine-rich repeats, the first PKD domain and the C-type lectin motif, and 2179 amino acids at the C-terminus, which would include the REJ domain, the transmembrane region, and the cytoplasmic region. We speculated, therefore, that the smaller of the two blobs is at the N-terminus, whereas the larger blob is at the C-terminus, with the intervening strings being composed of the 15 tandem PKD domains, as illustrated in Figure 2G. The reverse arrangement makes much less sense with respect to the known location of domains within PC1.

WT PC1 Purified via the C-Terminal HA Tag. To clarify the relationship between the blobs and the sequence of PC1, we next examined WT PC1. The protein was first isolated by

dx.doi.org/10.1021/bi300134b | *Biochemistry* 2012, 51, 2879–2888

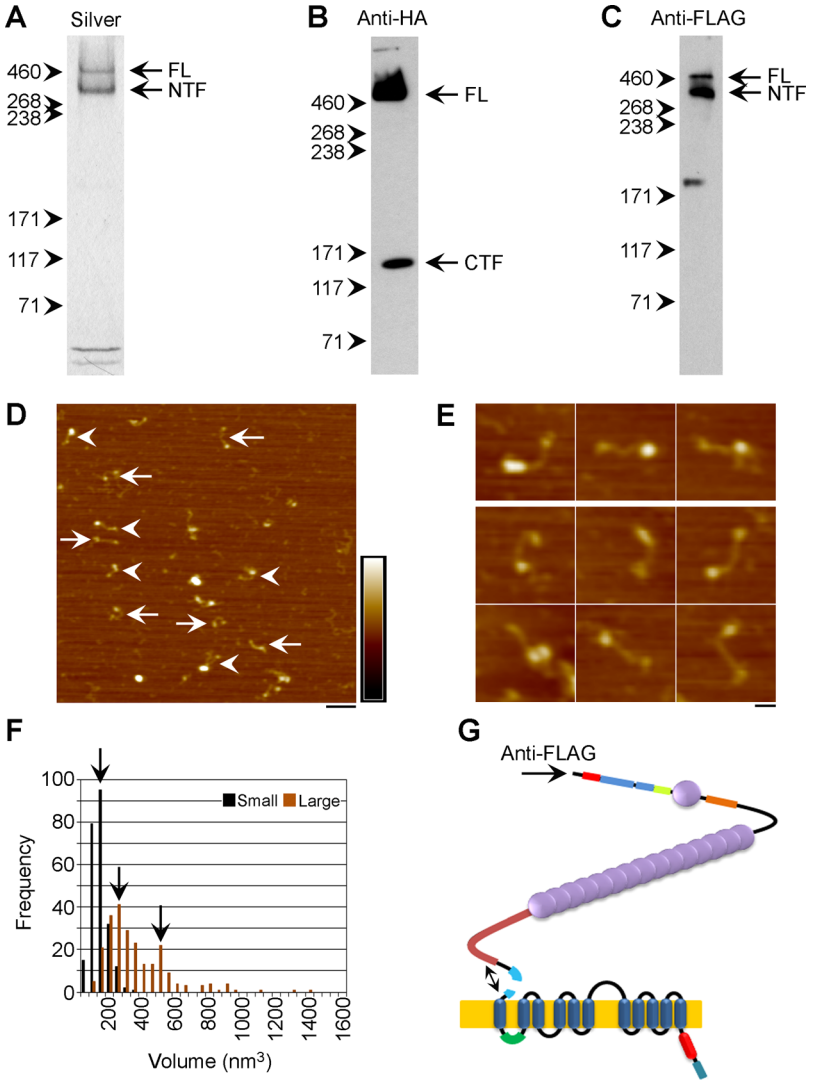

Figure 4. AFM imaging of WT PC1 isolated using anti-FLAG immunobeads. Protein was isolated by immunoaffinity chromatography, using anti-FLAG immunobeads, followed by elution with FLAG peptide. Isolated protein was analyzed by silver staining (A) or immunoblotting using mouse monoclonal anti-HA (B) or anti-FLAG (C) antibodies. (D) Low-magnification AFM image of isolated proteins. Asymmetric blob–string–blob structures are indicated by the arrowheads; structures with more equally sized blobs are indicated by the arrows. Horizontal scale bar, 100 nm. Color-height scale, 0–5 nm. (E) Gallery of zoomed images of blob–string–blob structures. The top three panels show representative asymmetric structures, while the bottom six panels show structures with more equally sized blobs. Horizontal scale bar, 25 nm. (F) Frequency distributions of molecular volumes of small and large blobs. Arrows indicate volume peaks. (G) Schematic illustration of the isolated protein, indicating the epitope tag used for affinity purification.

anti-HA immunoaffinity chromatography followed by elution with the HA peptide. A silver-stained SDS–polyacrylamide gel of the isolated sample is shown in Figure 3A. Two major bands are present, at 460 and 130 kDa. Given their sizes, these bands must represent the FL protein and the C-terminal fragment (CTF), produced by cleavage at the GPS site, and pulled out by the anti-HA antibody. Consistent with this interpretation, both the 460 kDa band and the 130 kDa band were detected on an immunoblot with an anti-HA antibody (Figure 3B). An anti-FLAG blot of the sample (Figure 3C) showed the 460 kDa band (the FL protein) and a faint band running at 320 kDa, which is likely to represent a small amount of the N-terminal fragment (NTF) that copurified with the CTF but was not detected by silver staining.

WT PC1 isolated using the anti-HA beads was imaged by AFM. A representative low-magnification image is shown in Figure 3D, and a gallery of zoomed images is shown in Figure 3E. As with the GPS cleavage mutant, the images show a number of structures consisting of pairs of unequally sized blobs connected by a string (arrowheads in Figure 3D) and occasional single blobs. This result is consistent with the interpretation detailed above: the anti-HA immunobeads should isolate both FL protein, which should appear identical to the FL GPS cleavage mutant, and also the CTF, which should contain the transmembrane region and the cytoplasmic tail. Frequency distributions of the smaller and larger blobs within the structures are shown in Figure 3F. The mean volumes for the smaller and larger particles, from separate Gaussian fits, were 120 ± 3 and 480 ± 11 nm^3 (n = 236), respectively, similar to the values for the GPS cleavage mutant. Interestingly, there appeared to be a small peak at about 220 nm^3, which may represent the NTF which has been copurified with the CTF after GPS cleavage (see Figure 3G); however, this was not statistically significant (see below). The C-terminal

dx.doi.org/10.1021/bi300134b | *Biochemistry* 2012, 51, 2879–2888

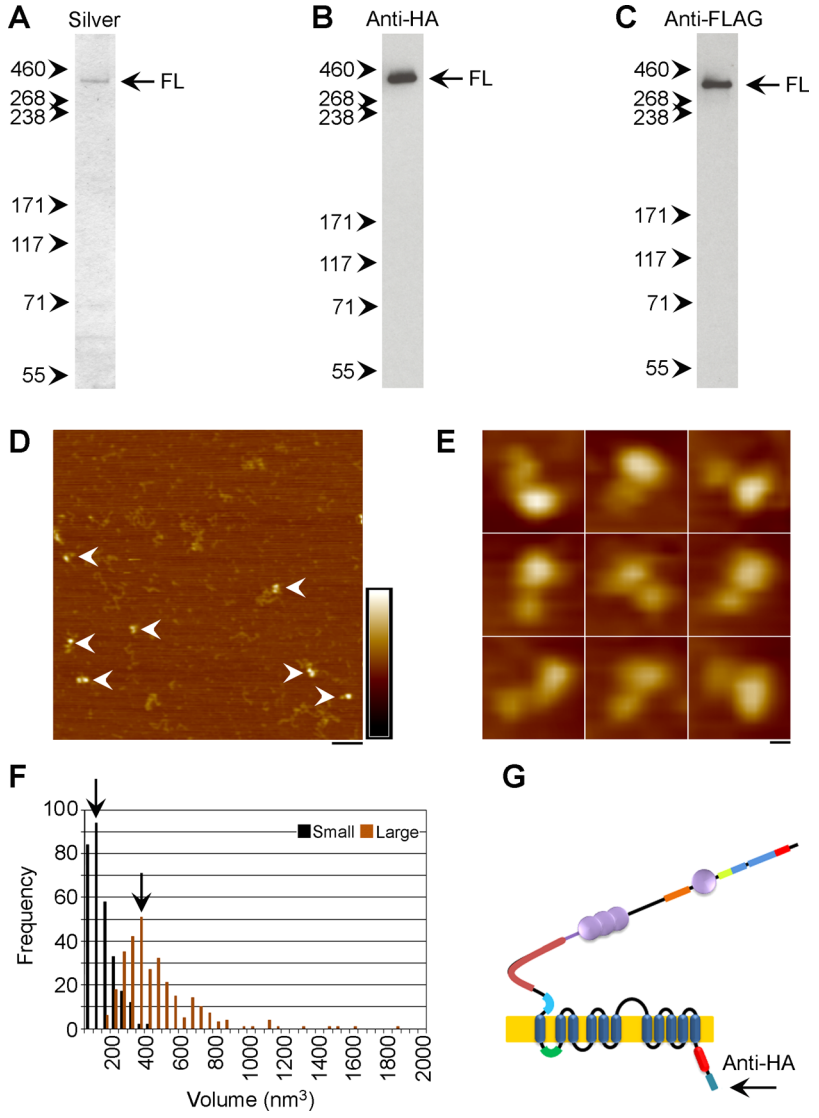

Figure 5. Isolation and AFM imaging of PC1 deletion mutant 1. Protein was isolated by immunoaffinity chromatography, using anti-HA immunobeads, followed by elution with HA peptide. Isolated protein was analyzed by silver staining (A) or immunoblotting using mouse monoclonal anti-HA (B) or anti-FLAG (C) antibodies. (D) Low-magnification AFM image of isolated proteins. Asymmetric double-blob structures are indicated by the arrowheads. Horizontal scale bar, 100 nm. Color-height scale, 0–5 nm. (E) Gallery of zoomed images of double-blob structures. Horizontal scale bar, 10 nm. (F) Frequency distributions of molecular volumes of small and large blobs. Arrows indicate volume peaks. (G) Schematic illustration of the isolated protein, indicating the epitope tag used for affinity purification.

part of the NTF should contain only the REJ domain, which comprises ~900 amino acids, and should therefore have a molecular mass of 99 kDa and a molecular volume of ~187 nm^3, close to the observed size (eq 2). The mean string length for WT PC1 was 35.0 ± 0.6 nm (n = 236). According to its crystal structure, the length of a single PKD domain is ~4.8 nm;[26] so 15 PKD domains laid end to end would be 72 nm long. It is possible, therefore, that some of the PKD domains are incorporated into the blobs; alternatively, the PKD domains might not be arranged in a simple linear, end-to-end array.

WT PC1 Purified via the N-Terminal FLAG Tag. When WT PC1 was immunopurified using anti-FLAG beads, a different pattern of bands was seen, as shown in Figure 4A–C. The silver stain (Figure 4A) now showed the FL protein (460 kDa) and the NTF (320 kDa). The anti-HA blot (Figure 4B) showed the FL protein and the CTF (copurified with the NTF but too faint to detect on the silver stain); the anti-FLAG blot (Figure 4C) showed the FL protein and a strong band corresponding to the NTF. We cannot identify the smaller band running at around 190 kDa.

When WT PC1 isolated using the anti-FLAG immunobeads was imaged by AFM, two types of particle could be seen on the low-magnification images (e.g., Figure 4D): particles with the characteristic pairs of unequally sized blobs (arrowheads) and, more commonly, particles with more equally sized blobs (arrows). Examples of the two types of particles are shown in the gallery in Figure 4E. Frequency distributions for the smaller and larger blobs are shown in Figure 4F. The mean volume of the smaller particle is 108 ± 1 nm^3 (n = 235), close to the value for the smaller particle in the HA isolation (above); however, the 469 ± 6 nm^3 (n = 74) peak for the large particle is less heavily populated than before, and the 223 ± 4 nm^3 (n = 161) peak (mentioned above) is now dominant (data fitted by a double Gaussian). If the majority of the WT PC1 undergoes GPS cleavage, as appears to be the case in this experiment, according to the relative densities of the silver stained bands

dx.doi.org/10.1021/bi300134b | Biochemistry 2012, 51, 2879–2888

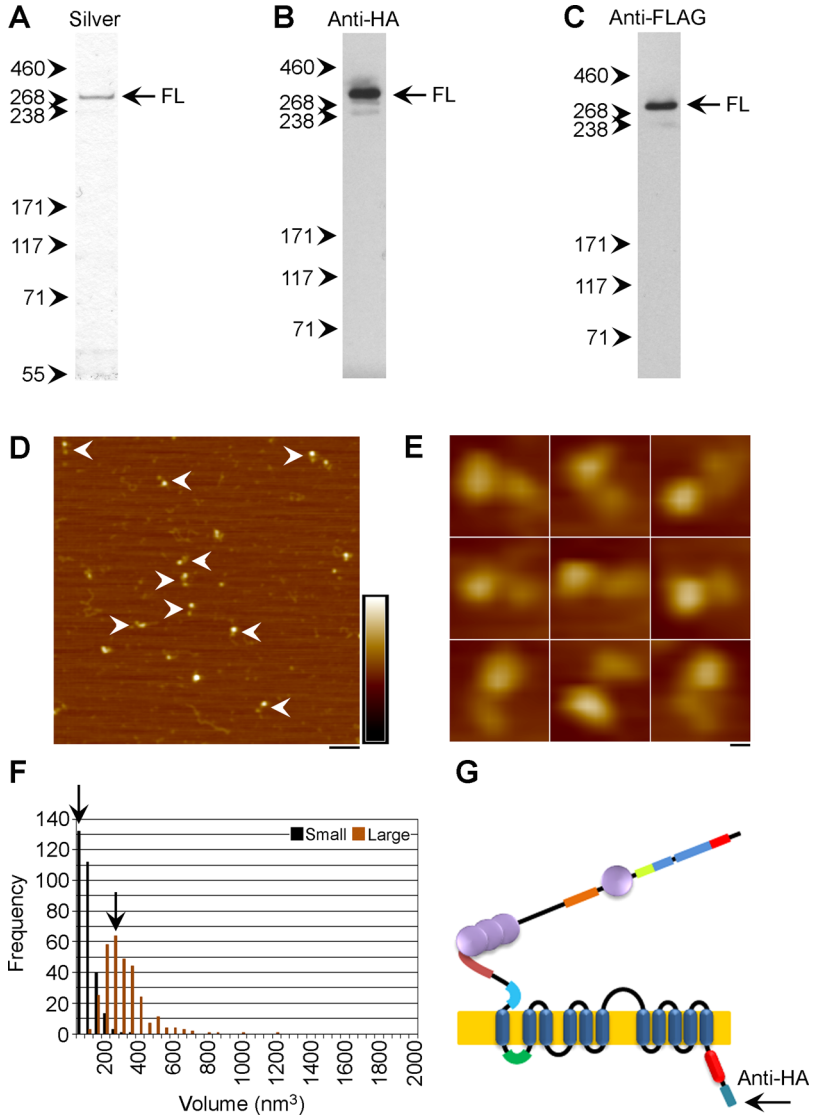

Figure 6. Isolation and AFM imaging of PC1 deletion mutant 2. Protein was isolated by immunoaffinity chromatography, using anti-HA immunobeads, followed by elution with HA peptide. Isolated protein was analyzed by silver staining (A) or immunoblotting using mouse monoclonal anti-HA (B) or anti-FLAG (C) antibodies. (D) Low-magnification AFM image of isolated proteins. Asymmetric double-blob structures are indicated by the arrowheads. Horizontal scale bar, 100 nm. Color-height scale, 0−5 nm. (E) Gallery of zoomed images of double-blob structures. Horizontal scale bar, 10 nm. (F) Frequency distributions of molecular volumes of small and large blobs. Arrows indicate volume peaks. (G) Schematic illustration of the isolated protein, indicating the epitope tag used for affinity purification.

(Figure 4A), then the major species pulled out by the anti-FLAG beads should be the NTF, with a ~200 nm^3 larger blob, as is seen (Figure 4G). The 469 nm^3 blob likely represents uncleaved PC1 that is also isolated by the immunobeads.

PC1 Deletion Mutant 1. To shed light on the relationship between the stringlike structure and the tandem PKD domains, a deletion mutant of the PC1 GPS cleavage mutant lacking residues N1188-E2103, representing PKD domains 6−15 and parts of PKD domains 5 and 16 (deletion mutant 1), was expressed in tsA 201 cells and purified using anti-HA affinity chromatography. The silver stain (Figure 5A) showed a protein of molecular mass 360 kDa that reacted with both anti-HA (Figure 5B) and anti-FLAG antibodies (Figure 5C) on immunoblots. AFM imaging of the isolated protein revealed pairs of unequally sized blobs with no intervening strings (arrowheads in Figure 5D). Examples of the particles are shown in the gallery in Figure 5E. Frequency distributions for the smaller and larger blobs are shown in Figure 5F. The mean volume of the smaller particle was now 49 ± 5 nm^3 (n = 301), in contrast to the 105 nm^3 for the FL protein, and the larger particle was also smaller (327 ± 8 nm^3 compared with 544 nm^3 for the FL protein). These results are consistent with the above suggestion that some PKD domains at the ends of the tandem repeat are included in the blobs, although it is also possible that the deletion of a central part of the protein might have caused some destabilization of the structure of the N- and/or C-termini. The structure of the truncated protein is illustrated in Figure 5G.

PC1 Deletion Mutant 2. To further probe the composition of the molecule, a deletion mutant of the PC1 GPS cleavage mutant lacking residues T1118-R2691, representing PKD domains 5−16, and most of the REJ domain (deletion mutant 2), was expressed in tsA 201 cells and purified using anti-HA affinity chromatography. The silver stain (Figure 6A) showed a protein of molecular mass 290 kDa that reacted with both anti-HA (Figure 6B) and anti-FLAG antibodies (Figure 6C) on

dx.doi.org/10.1021/bi300134b | *Biochemistry* 2012, 51, 2879−2888

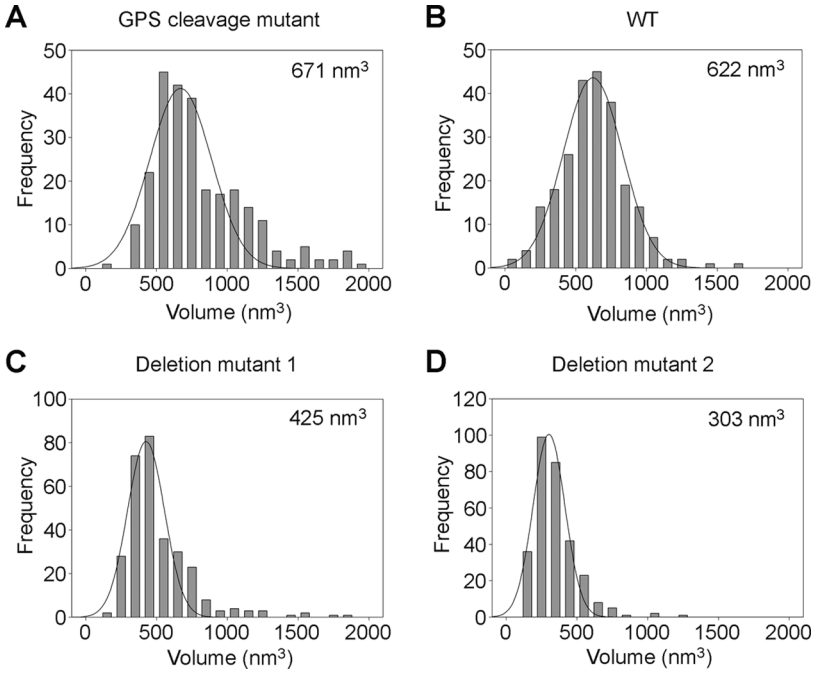

Figure 7. Total particle volumes for the various constructs. Frequency distributions of summed molecular volumes for large and small blobs within individual particles were constructed for the PC1 GPS cleavage mutant (A), WT PC1 (B), deletion mutant 1 (C), and deletion mutant 2 (D). Curves indicate the fitted Gaussian functions. The means of the distributions are indicated.

immunoblots. AFM imaging of the isolated protein again revealed pairs of unequally sized blobs with no intervening strings (arrowheads in Figure 6D). Examples of the particles are shown in the gallery in Figure 6E. Frequency distributions for the smaller and larger blobs are shown in Figure 6F. The mean volume for the smaller particle was now reduced even further to 38 ± 1 nm^3 (n = 301), in comparison with deletion mutant 1, and the larger particle was also smaller (241 ± 4 nm^3 compared with 544 nm^3 for the full-length protein). These results further support the suggestion that some PKD domains are included in the blobs and also indicate that the REJ domain contributes to the larger blob. The domain architecture of the truncated protein is illustrated in Figure 6G.

Summed Particle Sizes for the Various Constructs. For all four constructs, the combined particle sizes were calculated and frequency distributions of volumes were produced. The results are shown in Figure 7. The peak molecular volumes for the GPS mutant and the WT protein (purified via its HA tag) were very similar: 671 ± 23 nm^3 (n = 259; Figure 7A) and 622 ± 8 nm^3 (n = 236; Figure 7B), respectively. In contrast, the peak volume for deletion mutant 1 was significantly reduced, to 425 ± 11 nm^3 (n = 301; Figure 7C), and the peak volume for deletion mutant 2 was reduced still further, to 303 ± 6 nm^3 (n = 301; Figure 7D). Notably, these volumes are in similar proportions to the molecular masses of the constructs 460 kDa for WT protein and the GPS cleavage mutant, 360 kDa (80% of full length) for deletion mutant 1, and 290 kDa (63% of full length) for deletion mutant 2.

DISCUSSION

PC1 is highly expressed in renal tubular cells, with the highest levels found in the collecting ducts (reviewed in ref 1). It is also expressed in other epithelia, including bile ducts and pancreatic ducts. At the subcellular level, PC1 is present in several different locations in renal epithelial cells; for instance, it is found at cell adhesion junctions and focal adhesions,[27−29] suggesting an involvement in cell−cell and cell−matrix adhesion. Most interestingly, PC1 is also localized to the primary cilium, along with PC2.[8−10] The primary cilium consists of membrane surrounding a core of microtubules (reviewed in ref 30). In cell culture models, mechanical or flow-induced deformation of the primary cilium results in an increase in intracellular Ca^{2+};[10] furthermore, the Ca^{2+} response is abolished in cells lacking PC1. These results indicate a role for the polycystin complex in flow sensing in the nephron. The expression of PC1 in adhesion complexes,[28,29] which are known to be exposed to mechanical stresses, further suggests that it might function as a polymodal mechanosensor.

Our results represent the first direct visualization of the structure of PC1 and reveal the architecture of the protein, with intriguing implications for its function. The REJ domain of PC1 likely protrudes into the extracellular medium from the membrane-spanning region as a globular domain. This structure acts as an anchor for a stringlike region composed of the tandem PKD domains. Our experiments reveal that the PKD domains do not assemble as a stiff rodlike structure, but rather form an easily deformable linker, which positions the globular N-terminus about 35 nm away from the host membrane.

The intracellular regions of PC1, including the C-terminus, are involved in a variety of important cell signaling pathways.[21,22,31−33] It has also been reported that the coiled-coil domain at the C-terminus interacts with a similar domain at the distal end of PC2 to form a calcium channel.[7,34] Dysfunction of this complex appears to lie at the heart of ADPKD. Thus, both by itself and in association with PC2, PC1 has the ability to operate in a number of signaling cascades; however, the trigger for activation of these cascades is unknown. On the basis of our visualization of the structure of PC1 structure, we hypothesize that the N-terminal globular domain binds specific targets. This binding may generate a physical force, resulting in the

deformation of the string domain and consequent changes in signaling via the intracellular region. The flexibility of the PKD repeats would suggest that deformation occurs in the manner of a spring being stretched, rather than a stiff rod being bent. This suggestion is consistent with single-molecule force measurements showing that tandem PKD domains have extraordinary mechanical strength along the domain axis.[35−37]

PC1 might function to attach the host cell membrane to an adjacent cell across a cell−cell junction or to the extracellular matrix. There is evidence that the C-type lectin domain, present close to the N-terminus of the protein, is able to bind collagens type I, II, and IV in a Ca^{2+}-dependent manner,[38] while the leucine-rich repeats, also found near the N-terminus, bind collagen, fibronectin, and laminin.[39] Furthermore, it has been shown that the PKD domains themselves undergo high-affinity, Ca^{2+}-independent homophilic interactions and that anti-PKD domain antibodies disrupt cell−cell interactions in Madin−Darby canine kidney (MDCK) cell monolayers.[29] Intriguingly, proteins containing tandem PKD-like domains have been identified in the surface layer of the archaeobacterium *Methanosarcina mazei*, which grows in well-defined multicellular structures,[40] suggesting that a cell−cell adhesion function for PKD-containing proteins might be ancient.

It is less obvious how protein−protein interactions involving PC1 might contribute to flow sensing by the primary cilium. The length of the linker likely precludes an interaction with targets on other cells; hence, any binding partner must be either on the same primary cilium or within the lumen of the nephron. One possibility is that the N-terminus of PC1 binds to the membrane of the primary cilium; the PKD domains, lying parallel to the membrane, would then be stretched and contracted by bending of the cilium by fluid flow. Alternatively, the N-terminus could mediate an association between the primary cilium and urinary exosomes, which have themselves been reported to contain considerable amounts of PC1.[16,41]

PC1 belongs to a growing family of proteins that possess a similar overall structure, including a large N-terminus, a GPS cleavage site and 11 transmembrane domains (reviewed in ref 11). However, regions that we have identified as important in the overall architecture, in particular the tandem PKD repeats, are most abundant in PC1, and some family members lack these repeats altogether. PC1 is a putative mechanosensor, whereas PKD1L3, which has no PKD domains, is suggested to function as an acid taste receptor.[42] Interestingly, PKD1L1, which possesses two PKD domains, has recently been shown to interact with PC2.[43] Furthermore, it has been suggested that this complex contributes to mechanosensation by motile cilia during the determination of left−right axis asymmetry.[44]

In the current study, we have purified several PC1 constructs, including the full-length WT protein, and used AFM to directly visualize the architecture of the protein. It is clear that PC1 directly interacts with PC2. We therefore expect that single-molecule imaging by AFM should provide a powerful method for determining the structure of the complete polycystin complex. This information, in turn, should provide significant insights into the etiology of ADPKD.

■ ASSOCIATED CONTENT

Supporting Information

Immunofluorescence analysis of the expression of PC1 constructs in tsA 201 cells. This material is available free of charge via the Internet at http://pubs.acs.org.

■ AUTHOR INFORMATION

Corresponding Author

*Phone: +44 1223 334014; Fax: +44 1223 334100; e-mail: jme1000@cam.ac.uk.

Funding

A.P.S. is a member of the University of Cambridge MB/PhD Programme and is supported by the Jean Shanks Foundation and the James Baird Fund. This work was supported by Kidney Research UK.

Notes

The authors declare no competing financial interest.

■ ACKNOWLEDGMENTS

We are very grateful to Dr. M. J. Caplan (Yale University) for providing the WT and GPS cleavage mutant constructs of PC1 and to the Cambridge Institute of Medical Research Proteomics Core for protein identification.

■ ABBREVIATIONS

AFM, atomic force microscopy; ADPKD, autosomal dominant polycystic kidney disease; CTF, C-terminal fragment; ER, endoplasmic reticulum; FL, full length; GPS, G protein-coupled receptor proteolytic site; HA, hemagglutinin; NTF, N-terminal fragment; PC, polycystin; PLAT, polycystin−lipoxygenase−alphatoxin; REJ, receptor for egg jelly; SPIP, Scanning Probe Image Processor; TRP, transient receptor potential; SEM, standard error of the mean; WSC, cell wall integrity and stress response component; WT, wild type.

■ REFERENCES

(1) Yoder, B. K., Mulroy, S., Eustace, H., Boucher, C., and Sandford, R. (2006) Molecular pathogenesis of autosomal dominant polycystic kidney disease. *Exp. Rev. Mol. Med. 8*, 1−22.

(2) Harris, P. C., and Torres, V. E. (2009) Polycystic kidney disease. *Annu. Rev. Med. 60*, 27.1−27.17.

(3) Chapin, H. C., and Caplan, M. J. (2010) The cell biology of polycystic kidney disease. *J. Cell Biol. 191*, 701−710.

(4) Hughes, J., Ward, C. J., Peral, B., Aspinwall, R., Clark, K., San Millán, J. L., Gamble, V., and Harris, P. C. (1995) The polycystic kidney disease 1 (PKD1) gene encodes a novel protein with multiple cell recognition domains. *Nat. Genet. 10*, 151−160.

(5) The International Polycystic Kidney Disease Consortium (1995) Polycystic kidney disease: the complete structure of the PKD1 gene and its protein. *Cell 81*, 289−298.

(6) Mochizuki, T., Wu, G., Hayashi, T., Xenophontos, S. L., Veldhuisen, B., Saris, J. J., Reynolds, D. M., Cai, Y., Gabow, P. A., Pierides, A., Kimberling, W. J., Breuning, M. H., Deltas, C. C., Peters, D. J., and Somlo, S. (1996) PKD2, a gene for polycystic kidney disease that encodes an integral membrane protein. *Science 272*, 1339−1342.

(7) Hanaoka, K., Qian, F., Boletta, A., Bhunia, A. K., Piontek, K., Tsiokas, L., Sukhatme, V. P., Guggino, W. B., and Germino, G. G. (2000) Co-assembly of polycystin-1 and -2 produces unique cation-permeable currents. *Nature 408*, 990−994.

(8) Barr, M. M., and Sternberg, P. W. (1999) A polycystic kidney-disease gene homologue required for male mating behaviour in *C. elegans*. *Nature 410*, 386−389.

(9) Yoder, B. K., Hou, X., and Guay-Woodford, L. M. (2002) The polycystic kidney disease proteins, polycystin-1, polycystin-2, polaris, and cystin, are co-localized in renal cilia. *J. Am. Soc. Nephrol. 13*, 2508−2516.

(10) Nauli, S. M., Alenghat, F. J., Luo, Y., Williams, E., Vassilev, P. M., Li, X., Elia, A. E. H., Lu, W., Brown, E. M., Quinn, S. J., Ingber, D. E., and Zhou, J. (2003) Polycystins 1 and 2 mediate mechanosensation in the primary cilium of kidney cells. *Nat. Genet. 33*, 129−137.

(11) Zhou, J. (2009) Polycystins and primary cilia: primers for cell cycle progression. *Annu. Rev. Physiol. 71*, 83−113.
(12) Delmas, P., Nauli, S. M., Li, X., Coste, B., Osorio, N., Crest, M., Brown, D. A., and Zhou, J. (2004) Gating of the polycystin ion channel signaling complex in neurons and kidney cells. *FASEB J. 18*, 740−742.
(13) Geng, L., Boehmerle, W., Maeda, Y., Okuhara, D. Y., Tian, X., Yu, Z., Choe, C.-U., Anyatonwu, G. I., Ehrlich, B. E., and Somlo, S. (2008) Syntaxin 5 regulates the endoplasmic reticulum channel-release properties of polycystin-2. *Proc. Natl. Acad. Sci. U. S. A. 105*, 15920−15925.
(14) Wegierski, T., Steffl, D., Kopp, C., Tauber, R., Buchholz, B., Nitschke, R., Kuehn, E. W., Walz, G., and Köttgen, M. (2009) TRPP2 channels regulate apoptosis through the Ca^{2+} concentration in the endoplasmic reticulum. *EMBO J. 28*, 490−499.
(15) Qian, F., Boletta, A., Bhunia, A. K., Xu, H., Ahrabi, A. K., Watnick, T. J., Zhou, F., and Germino, G. G. (2002) Cleavage of polycystin-1 requires the receptor for egg jelly domain and is disrupted by human autosomal-dominant polycystic kidney disease 1-associated mutations. *Proc. Natl. Acad. Sci. U. S. A. 99*, 16981−16986.
(16) Hogan, M. C., Manganelli, L., Woollard, J. R., Masyuk, A. I., Masyuk, T. V., Tammachote, R., Huang, B. Q., Leontovich, A. A., Beito, T. G., Madden, B. J., Charlesworth, M. C., Torres, V. E., LaRusso, N. F., Harris, P. C., and Ward, C. J. (2009) Characterization of PKD protein-positive exosome-like vesicles. *J. Am. Soc. Nephrol. 20*, 278−288.
(17) Wei, W., Hackmann, K., Xu, H., Germino, G., and Qian, F. (2007) Characterization of *cis*-autoproteolysis of polycystin-1, the product of human polycystic kidney disease 1 gene. *J. Biol. Chem. 282*, 21729−21737.
(18) Qian, F., Germino, F. J., Cai, Y., Zhang, X., Somlo, S., and Germino, G. G. (1997) PKD1 interacts with PKD2 through a probable coiled-coil domain. *Nat. Genet. 16*, 179−183.
(19) Tsiokas, L., Kim, E., Arnould, T., Sukhatme, V. P., and Walz, G. (1997) Homo and heterodimeric interactions between the gene products of PKD1 and PKD2. *Proc. Natl. Acad. Sci. U. S. A. 94*, 6965−6970.
(20) Yu, S., Hackmann, K., Gao, J., He, X., Piontek, K., García González, M. A., Menezes, L. F., Xu, H., Germino, G. G., Zuo, J., and Qian, F. (2007) Essential role of cleavage of polycystin-1 at G protein-coupled receptor proteolytic site for kidney tubular structure. *Proc. Natl. Acad. Sci. U. S. A. 104*, 18688−18693.
(21) Chauvet, V., Tian, X., Husson, H., Grimm, D. H., Wang, T., Hiesenberger, T., Igarashi, P., Bennett, A. M., Ibraghimov-Beskrovnaya, O., Somlo, S., and Caplan, M. J. (2004) Mechanical stimuli induce cleavage and nuclear translocation of the polycystin-1 C terminus. *J. Clin. Invest. 114*, 1433−1443.
(22) Low, S. H., Vasanth, S., Larson, C. H., Mukherjee, S., Sharma, N., Kinter, M. T., Kane, M. E., Obara, T., and Weimbs, T. (2006) Polycystin-1, STAT6, and P100 function in a pathway that transduces ciliary mechanosensation and is activated in polycystic kidney disease. *Dev. Cell 10*, 57−69.
(23) Grimm, D. H., Cai, Y., Chauvet, V., Rajendran, V., Zeltner, R., Geng, L., Avner, E. D., Sweeney, W., Somlo, S., and Caplan, M. J. (2003) Polycystin-1 distribution is modulated by polycystin-2 expression in mammalian cells. *J. Biol. Chem. 278*, 36786−36793.
(24) Schneider, S. W., Lärmer, J., Henderson, R. M., and Oberleithner, H. (1998) Molecular weights of individual proteins correlate with molecular volumes measured by atomic force microscopy. *Pflügers Arch. 435*, 362−367.
(25) Neaves, K. J., Cooper, L. P., White, J. H., Carnally, S. M., Dryden, D. T. F., Edwardson, J. M., and Henderson, R. M. (2009) Atomic force microscopy of the EcoKI type I DNA restriction enzyme bound to DNA shows enzyme dimerisation and DNA looping. *Nucleic Acids Res. 37*, 2053−2063.
(26) Bycroft, M., Bateman, A., Clarke, J., Hamill, S. J., Sandford, R., Thomas, R. L., and Chothia, C. (1999) The structure of a PKD domain from polycystin-1: implications for polycystic kidney disease. *EMBO J. 18*, 297−305.
(27) Wilson, P. D., Geng, L., Li, X. H., and Burrow, C. R. (1999) The PKD1 gene product, "polycystin-1", is a tyrosine-phosphorylated protein that colocalizes with alpha2beta1-integrin in focal clusters in adherent renal epithelia. *Lab. Invest. 79*, 1311−1323.
(28) Peters, D. J. M., van de Wal, A., Spruit, L., Saris, J. J., Breuning, M. H., Bruijn, J. A., and de Heer, E. (1999) Cellular colocalization and tissue distribution of polycystin-1. *J. Pathol. 188*, 439−446.
(29) Ibraghimov-Beskrovnaya, O., Bukanov, N. O., Donohue, L. C., Dackowski, W. R., Klinger, K. W., and Landes, G. M. (2000) Strong homophilic interactions of the Ig-like domains of polycystin-1, the protein product of an autosomal dominant polycystic kidney disease gene, PKD1. *Hum. Mol. Genet. 9*, 1641−1649.
(30) Praetorius, H. A., and Spring, K. R. (2005) A physiological view of the primary cilium. *Annu. Rev. Physiol. 67*, 515−529.
(31) Bhunia, A. K., Piontek, K., Boletta, A., Liu, L., Qian, F., Xu, P. N., Germino, F. J., and Germino, G. G. (2002) PKD1 induces p21(waf1) and regulation of the cell cycle via direct activation of the JAK-STAT signaling pathway in a process requiring PKD2. *Cell 109*, 157−168.
(32) Puri, S., Magenheimer, B. S., Maser, R. L., Ryan, E. M., Zien, C. A., Walker, D. D., Wallace, D. P., Hempson, S. J., and Calvet, J. P. (2004) Polycystin-1 activates the calcineurin/NFAT (nuclear factor of activated T-cells) signaling pathway. *J. Biol. Chem. 279*, 55455−55464.
(33) Yu, W., Ritchie, B. J., Su, X., Zhou, J., Meigs, T. E., and Denker, B. M. (2011) Identification of polycystin-1 and Gα12 binding regions necessary for regulation of apoptosis. *Cell Signal. 23*, 213−221.
(34) Giamarchi, A., Feng, S., Rodat-Despoix, L., Xu, Y., Bubenshchikova, E., Newby, L. J., Hao, J., Gaudioso, C., Crest, M., Lupas, A. N., Honoré, E., Williamson, M. P., Obara, T., Ong, A. C., and Delmas, P. (2010) A polycystin-2 (TRPP2) dimerization domain essential for the function of heteromeric polycystin complexes. *EMBO J. 29*, 1176−1191.
(35) Forman, J. R., Qamar, S., Paci, E., Sandford, R. N., and Clarke, J. (2005) The remarkable mechanical strength of polycystin-1 supports a direct role in mechanotransduction. *J. Mol. Biol. 349*, 861−871.
(36) Forman, J. R., Yew, Z. T., Qamar, S., Sandford, R. N., Paci, E., and Clarke, J. (2009) Non-native interactions are critical for mechanical strength in PKD domains. *Structure 17*, 1582−1590.
(37) Ma, L., Xu, M., and Oberhauser, A. F. (2010) Naturally occurring osmolytes modulate the nanomechanical properties of polycystic kidney disease domains. *J. Biol. Chem. 285*, 38438−38443.
(38) Weston, B. S., Bagnéris, C., Price, R. G., and Stirling, J. L. (2001) The polycystin-1 C-type lectin domain binds carbohydrate in a calcium-dependent manner, and interacts with extracellular matrix proteins in vitro. *Biochim. Biophys. Acta 1536*, 161−176.
(39) Malhas, A. N., Abuknesha, R. A., and Price, R. G. (2002) Interaction of the leucine-rich repeats of polycystin-1 with extracellular matrix proteins: possible role in cell proliferation. *J. Am. Soc. Nephrol. 13*, 19−26.
(40) Jing, H., Takagi, J., Liu, J.-H., Lindgren, S., Zhang, R.-G., Joachimiak, A., Wang, J.-H., and Springer, T. (2002) Archaeal surface layer proteins contain β propeller, PKD, and β helix domains and are related to metazoan cell surface proteins. *Structure 10*, 1453−1464.
(41) Pisitkun, T., Shen, R. F., and Knepper, M. A. (2004) Identification and proteomic profiling of exosomes in human urine. *Proc. Natl. Acad. Sci. U. S. A. 101*, 13368−13373.
(42) Ishimaru, Y., Inada, H., Kubota, M., Zhuang, H., Tominaga, M., and Matsunami, H. (2006) Transient receptor potential family members PKD1L3 and PKD2L1 form a candidate sour taste receptor. *Proc. Natl. Acad. Sci. U. S. A. 103*, 12569−12574.
(43) Field, S., Riley, K. L., Grimes, D. T., Hilton, H., Simon, M., Powles-Glover, N., Siggers, P., Bogani, D., Greenfield, A., and Norris, D. P. (2011) Pkd1l1 establishes left-right asymmetry and physically interacts with Pkd2. *Development 138*, 1131−1142.
(44) Kamura, K., Kobayashi, D., Uehara, Y., Koshida, S., Iijima, N., Kudo, A., Yokoyama, T., and Takeda, H. (2011) Pkd1l1 complexes with Pkd2 on motile cilia and functions to establish the left-right axis. *Development 138*, 1121−1129.